Supplementary

Methods

MR image acquisition

MR images from patients from Shandong Cancer Hospital and Research Institute were obtained using a Philips 3.0 Tesla magnetic resonance scanner (Philips Medical Systems, the Netherlands) and a 6-channel head coil. Fast spin-echo sequences were routinely used to obtain high-resolution T1-weighted MPR sequences with the following parameters: TR =2.5 ms, TE =2.3 ms, slice thickness =5.0 mm, matrix size =512×512, and in-plane resolution =1.56×1.56 mm^2. The contrast-enhanced scan was performed 3–5 min after the intravenous injection of 0.1 mmol/kg contrast medium at a speed of 2 mL/s. The axial scanning parameters were as follows: TR =3.8 ms, TE =1.7 ms, matrix size =512×512, layer thickness =3.2 mm, and in-plane resolution =1.5×1.50 mm^2. The images from the axial scan were used to reconstruct the coronal and sagittal planes. The reconstruction parameters were as follows: matrix size =512×512, slice thickness =3.5 mm, and in-plane resolution =1.5×1.50 mm^2.

The MR images from the patients from Linyi People's Hospital were obtained by a 3.0 Tesla (Magnetom Tim/Trio; Siemens, Germany) magnetic resonance scanner and a 6-channel head coil. The scanning parameters for the T1-weighted sequence were as follows: TR =7.5 ms, TE =3.2 ms, thickness =3 mm, matrix size =512×512, and in-plane resolution =1.39×1.39 mm^2. Contrast medium (0.2 mL/kg) was injected intravenously at a speed of 2 mL/s; 2–4 min later, a contrast-enhanced scan was performed. The axial scanning parameters were as follows: TR =3.6 ms, TE =1.5 ms, matrix size =512×512, layer thickness =3.3 mm, and in-plane resolution =1.49×1.49 mm^2. The axial scan images were then used to reconstruct the coronal and sagittal planes using the following reconstruction parameters: matrix size =512×512, slice thickness =3.0 mm, and in-plane resolution =1.37×1.37 mm^2. However, the imaging parameters of the MR images from the TCIA varied, with the use of 1.5 Tesla and 3.0 Tesla MR scanners and various TR, TE, thickness, and in-plane resolution settings.

The principle of five-fold cross-validation

The principle of five-fold cross-validation is that the training set is randomly divided into 5 subsamples; 4 samples are used for model training, while a single subsample is retained to verify the trained model. The cross-validation was repeated 5 times, each subsample was validated once, and the average result was calculated (47).

Definition of indicators

As shown in Table S1, the following calculated indicators can be obtained:

(I) True negative (TN): the sample number indicates that it is a negative sample and is predicted to be a negative sample;

(II) False positive (FP): the sample number indicates that it is a negative sample and is predicted to be a positive sample;

(III) False negative (FN): the sample number indicates that it is a positive sample and is predicted to be a negative sample;

(IV) True positive (TP): the sample number indicates that it is a positive sample and is predicted to be a positive sample;

(V) $Accuracy = \frac{TP+TN}{TP+FN+FP+TN}$, the proportion of all correctly judged samples in all samples;

(VI) $Sensitivity = \frac{TP}{TP+FN}$, indicates the proportion of pairs in the positive sample;

(VII) $Specificity = \frac{TP}{TP+FP}$, indicates the proportion of pairs in a negative sample;

(VIII) $Precision / positive\ prediction\ value\left(PPV\right) = \frac{TP}{TP+FP}$, refers to the proportion of the true positive class among all the people who are judged to be positive;

(IX) $Negative\ predictive\ value\left(NPV\right) = \frac{TP}{TP+FN}$, refers to the proportion of the true negative class among all the people who are judged to be negative.

 https://dx.doi.org/10.21037/qims-21-722

Radiomics features

Before the feature extraction, images were discretised the method "fixed bin size". Besides, GLCM, GLRLM, GLSZM, GLDM, and NGTDM are 2D features, while shape features are 3D. During feature calculation, directions and pixel distance were employed with default settings. First-order texture statistics were based on the first-order histogram that describes distribution of voxel intensities in an image (31).

Table S1 Confusion matrix

Predicted class	Acted Class	
	1	0
1	TP	FP
0	FN	TN

Table S2 Three kinds of feature recursive elimination methods (SVM_RFE, LR_RFE and RF_RFE) were used to select the image group features extracted from the three single-plane MPR images, which were then combined and again subjected to the feature selection method

SVM_Combine	LR_Combine	Random forest_Combine
original_shape_Sphericity	original_glcm_Imc2	wavelet-LHH_glcm_Correlation
wavelet-HLL_firstorder_Mean	original_shape_Sphericity	wavelet-HLL_firstorder_Mean
wavelet-LHL_firstorder_Mean	wavelet-HLL_firstorder_Mean	wavelet-LLH_ngtdm_Contrast
wavelet-HHL_glcm_Imc2	original_shape_SurfaceVolumeRatio	wavelet-HLH_glcm_Correlation
wavelet-LLL_firstorder_Minimum	wavelet-HHL_glcm_Imc1	wavelet-LHL_firstorder_Mean
wavelet-HHH_firstorder_Median	wavelet-HLH_firstorder_Median	wavelet-LLH_ngtdm_Contrast
wavelet-LLH_glcm_Correlation	wavelet-HHH_gldm_DependenceNonUniformityNormalised	wavelet-LHL_firstorder_Mean
wavelet-HLH_firstorder_Median	wavelet-HLH_glcm_MCC	wavelet-HLH_glszm_LargeAreaEmphasis
original_glszm_GrayLevelNonUniformity	wavelet-LLL_firstorder_Skewness	wavelet-HLL_firstorder_Mean
original_glszm_GrayLevelNonUniformity	wavelet-LLL_firstorder_Minimum	wavelet-HLH_glcm_Correlation
wavelet-LHL_gldm_DependenceVariance	original_gldm_SmallDependenceLowGrayLevelEmphasis	wavelet-HLL_glrlm_RunEntropy
original_shape_Elongation	original_glszm_GrayLevelNonUniformity	
wavelet-HHH_firstorder_Median	wavelet-LHH_firstorder_Skewness	
wavelet-HHL_ngtdm_Contrast	original_glszm_GrayLevelNonUniformity	
wavelet-LHL_firstorder_Mean	original_shape_Elongation	
wavelet-LLH_firstorder_Kurtosis	wavelet-HHH_firstorder_Median	
wavelet-LLH_glcm_Idmn	wavelet-HHL_ngtdm_Contrast	
wavelet-LLH_firstorder_Skewness	wavelet-LLH_firstorder_Kurtosis	
wavelet-LHH_firstorder_Median	wavelet-LLH_glcm_Idmn	
Common features: wavelet-HLL_firstorder_Mean		

H: high pass filter; L: low pass filter. LR, logistic regression; SVM, support vector machine; RFE, recursive feature elimination.

 https://dx.doi.org/10.21037/qims-21-722

Table S3 Different single-plane MPR images, feature selection methods, classifiers, and deep learning feature extractors were employed to generate glioma grading models with cross-combinations of different deep learning and radiomics features, and their results were assessed with the training cohort

Model	Source of features	Train cohort					
		AUC	Accuracy	Sensitivity	Specificity	Precision	NPV
SVM	Radiomics-Axial	0.866±0.09	0.841	0.791	0.879	0.829	0.850
	Radiomics-Coronal	0.812±0.04	0.811	0.837	0.793	0.75	0.868
	Radiomics-Sagittal	0.927±0.03	0.871	0.884	0.862	0.826	0.909
	Radiomics-Combine	0.960±0.03	0.900	0.860	0.931	0.902	0.900
	VGG16-Axial	0.920±0.06	0.832	0.651	0.966	0.933	0.789
	VGG16-Coronal	0.895±0.038	0.772	0.767	0.776	0.717	0.818
	VGG16-Sagittal	0.963±0.016	0.921	0.837	0.983	0.973	0.891
	VGG16-Combine	0.967±0.030	0.911	0.837	0.966	0.947	0.889
	Radiomics+VGG16	0.927±0.055	0.832	0.744	0.897	0.842	0.825
	VGG19-Axial	0.859±0.097	0.811	0.581	0.983	0.962	0.760
	VGG19-Coronal	0.920±0.032	0.842	0.674	0.966	0.935	0.800
	VGG19-Sagittal	0.961±0.024	0.871	0.744	0.966	0.941	0.836
	VGG19-Combine	0.945±0.028	0.832	0.791	0.862	0.810	0.847
	[Radiomics+VGG19]-Combine	0.913±0.082	0.822	0.698	0.914	0.857	0.803
	Resnet-Axial	0.913±0.037	0.842	0.791	0.879	0.829	0.850
	Resnet-Coronal	0.942±0.054	0.881	0.860	0.897	0.840	0.897
	Resnet-Sagittal	0.950±0.034	0.881	0.814	0.931	0.897	0.871
	Resnet-Combine	0.933±0.060	0.901	0.837	0.948	0.923	0.887
	[Radiomics+Resnet]-Combine	0.896±0.053	0.703	0.349	0.966	0.882	0.667
	Xception-Axial	0.977±0.016	0.921	0.884	0.948	0.927	0.917
	Xception-Coronal	0.993±0.004	0.970	0.977	0.966	0.955	0.982
	Xception-Sagittal	0.978±0.015	0.970	0.977	0.966	0.955	0.982
	Xception-Combine	0.993±0.004	1.0	1.0	1.0	1.0	1.000
	[Radiomics+Xception]-Combine	0.983±0.017	0.931	0.884	0.966	0.950	0.918
	InceptionV3-Axial	0.977±0.020	0.941	0.907	0.966	0.951	0.933
	InceptionV3-Coronal	0.982±0.019	0.950	0.930	0.966	0.952	0.949
	InceptionV3-Sagittal	0.993±0.004	0.950	0.930	0.966	0.952	0.949
	InceptionV3-Combine	0.968±0.031	0.921	0.907	0.931	0.907	0.931
	[Radiomics+InceptionV3]-Combine	0.975±0.025	0.881	0.907	0.862	0.830	0.926
	InceptionResnetV2-Axial	0.770±0.055	0.732	0.767	0.707	0.660	0.804
	InceptionResnetV2-Coronal	0.960±0.032	0.901	0.884	0.914	0.884	0.914
	InceptionResnetV2-Sagittal	0.954±0.029	0.871	0.814	0.914	0.875	0.869
	InceptionResnetV2-Combine	0.957±0.042	0.891	0.837	0.931	0.900	0.885
	[Radiomics+InceptionResnetV2]-Combine	0.959±0.046	0.960	0.930	0.983	0.976	0.950
LR	Radiomics-Axial	0.898±0.069	0.792	0.630	0.914	0.844	0.768
	Radiomics-Coronal	0.893±0.088	0.832	0.814	0.845	0.795	0.860
	Radiomics-Sagittal	0.888±0.079	0.792	0.767	0.810	0.750	0.825
	Radiomics-Combine	0.919±0.054	0.881	0.837	0.914	0.878	0.883
	VGG16-Axial	0.897±0.062	0.812	0.791	0.828	0.773	0.842
	VGG16-Coronal	0.768±0.077	0.663	0.419	0.845	0.667	0.662
	VGG16-Sagittal	0.860±0.102	0.673	0.372	0.897	0.727	0.658
	VGG16-Combine	0.917±0.027	0.851	0.860	0.845	0.804	0.891
	[Radiomics+VGG16]-Combine	0.947±0.032	0.861	0.814	0.897	0.854	0.867
	VGG19-Axial	0.800±0.028	0.743	0.581	0.862	0.758	0.735
	VGG19-Coronal	0.872±0.144	0.792	0.744	0.828	0.762	0.814
	VGG19-Sagittal	0.933±0.015	0.822	0.791	0.844	0.791	0.845
	VGG19-Combine	0.937±0.037	0.871	0.791	0.931	0.895	0.857
	[Radiomics+VGG19]-Combine	0.947±0.047	0.911	0.884	0.931	0.905	0.915
	Resnet-Axial	0.849±0.068	0.752	0.674	0.810	0.725	0.770
	Resnet-Coronal	0.879±0.108	0.802	0.721	0.862	0.795	0.806
	Resnet-Sagittal	0.909±0.062	0.832	0.791	0.862	0.810	0.847
	Resnet-Combine	0.937±0.035	0.851	0.744	0.931	0.889	0.831
	[Radiomics+Resnet]-Combine	0.940±0.062	0.832	0.837	0.828	0.783	0.873
	Xception-Axial	0.967±0.026	0.901	0.837	0.948	0.923	0.887
	Xception-Coronal	0.958±0.039	0.910	0.860	0.948	0.925	0.902
	Xception-Sagittal	0.932±0.052	0.891	0.884	0.897	0.864	0.912
	Xception-Combine	0.952±0.053	0.901	0.860	0.931	0.902	0.900
	[Radiomics+Xception]-Combine	0.976±0.029	0.931	0.907	0.948	0.929	0.932
	InceptionV3-Axial	0.905±0.046	0.822	0.767	0.862	0.805	0.833
	InceptionV3-Coronal	0.950±0.024	0.842	0.767	0.897	0.846	0.839
	InceptionV3-Sagittal	0.889±0.087	0.812	0.698	0.897	0.833	0.800
	InceptionV3-Combine	0.959±0.448	0.901	0.907	0.897	0.867	0.929
	[Radiomics+InceptionV3]-Combine	0.972±0.041	0.921	0.884	0.948	0.927	0.917
	InceptionResnetV2-Axial	0.759±0.126	0.663	0.627	0.690	0.600	0.714
	InceptionResnetV2-Coronal	0.887±0.061	0.743	0.535	0.897	0.793	0.722
	InceptionResnetV2-Sagittal	0.827±0.136	0.772	0.744	0.793	0.727	0.807
	InceptionResnetV2-Combine	0.946±0.049	0.812	0.721	0.879	0.816	0.810
	[Radiomics+InceptionResnetV2]-Combine	0.984±0.011	0.931	0.907	0.948	0.929	0.932
Random Forest	Radiomics-Axial	0.824±0.073	0.752	0.651	0.828	0.737	0.762
	Radiomics-Coronal	0.811±0.095	0.772	0.674	0.845	0.763	0.778
	Radiomics-Sagittal	0.860±0.072	0.743	0.651	0.810	0.718	0.758
	Radiomics-Combine	0.824±0.084	0.733	0.628	0.810	0.711	0.746
	VGG16-Axial	0.678±0.084	0.634	0.465	0.759	0.588	0.657
	VGG16-Coronal	0.790±0.112	0.733	0.698	0.759	0.682	0.772
	VGG16-Sagittal	0.799±0.110	0.703	0.534	0.828	0.697	0.706
	VGG16-Combine	0.823±0.081	0.693	0.605	0.759	0.650	0.721
	Radiomics+VGG16	0.847±0.049	0.812	0.791	0.828	0.773	0.842
	VGG19-Axial	0.790±0.073	0.713	0.651	0.759	0.667	0.746
	VGG19-Coronal	0.818±0.112	0.743	0.651	0.810	0.718	0.758
	VGG19-Sagittal	0.690±0.107	0.703	0.651	0.741	0.651	0.741
	VGG19-Combine	0.865±0.086	0.802	0.674	0.897	0.829	0.788
	[Radiomics+VGG19]-Combine	0.845±0.084	0.772	0.698	0.828	0.750	0.769
	Resnet-Axial	0.906±0.074	0.861	0.767	0.931	0.892	0.844
	Resnet-Coronal	0.762±0.085	0.683	0.558	0.776	0.649	0.703
	Resnet-Sagittal	0.846±0.075	0.802	0.698	0.879	0.811	0.797
	Resnet-Combine	0.840±0.069	0.802	0.651	0.914	0.848	0.779
	[Radiomics+Resnet]-Combine	0.826±0.068	0.792	0.721	0.845	0.775	0.803
	Xception-Axial	0.839±0.091	0.792	0.698	0.862	0.789	0.794
	Xception-Coronal	0.884±0.058	0.792	0.698	0.862	0.789	0.794
	Xception-Sagittal	0.818±0.039	0.802	0.744	0.845	0.780	0.817
	Xception-Combine	0.898±0.048	0.792	0.744	0.828	0.762	0.814
	[Radiomics+Xception]-Combine	0.858±0.071	0.812	0.767	0.845	0.786	0.831
	InceptionV3-Axial	0.800±0.052	0.723	0.558	0.845	0.727	0.721
	InceptionV3-Coronal	0.858±0.064	0.802	0.674	0.897	0.829	0.788
	InceptionV3-Sagittal	0.664±0.142	0.663	0.372	0.879	0.696	0.654
	InceptionV3-Combine	0.811±0.064	0.713	0.581	0.810	0.694	0.723
	[Radiomics+InceptionV3]-Combine	0.846±0.068	0.782	0.721	0.828	0.756	0.800
	InceptionResnetV2-Axial	0.807±0.119	0.802	0.791	0.810	0.756	0.839
	InceptionResnetV2-Coronal	0.667±0.079	0.574	0.186	0.862	0.500	0.588
	InceptionResnetV2-Sagittal	0.832±0.057	0.733	0.581	0.845	0.735	0.731
	InceptionResnetV2-Combine	0.787±0.123	0.733	0.651	0.793	0.700	0.754
	[Radiomics+InceptionResnetV2]-Combine	0.873±0.078	0.762	0.721	0.793	0.721	0.793

LR, logistic regression; SVM, support vector machine; NPV, negative predictive value.

Table S4 Different single-plane MPR images, feature selection methods, classifiers, and deep learning feature extractors were employed to generate glioma grading models with cross-combinations of different deep learning and radiomics features, and their results were assessed with the test cohort

Model	Source of features	Test cohort							
		AUC	Accuracy	Sensitivity	Specificity	Precision	NPV	Number of features	Radiomics ratio
SVM	Radiomics-Axial	0.790	0.720	0.600	0.840	0.789	0.677	12	
	Radiomics-Coronal	0.788	0.780	0.720	0.840	0.818	0.750	19	
	Radiomics-Sagittal	0.686	0.680	0.800	0.560	0.645	0.737	19	
	Radiomics-Combine	0.822	0.740	0.760	0.720	0.731	0.750	19	
	VGG16-Axial	0.641	0.580	0.400	0.760	0.625	0.559	19	
	VGG16-Coronal	0.550	0.440	0.480	0.400	0.444	0.435	18	
	VGG16-Sagittal	0.612	0.480	0.440	0.520	0.478	0.481	19	
	VGG16-Combine	0.622	0.620	0.440	0.800	0.688	0.588	19	
	Radiomics+VGG16	0.792	0.680	0.640	0.720	0.696	0.667	17	10/17 (58.8%)
	VGG19-Axial	0.684	0.620	0.520	0.720	0.650	0.600	18	
	VGG19-Coronal	0.699	0.620	0.360	0.880	0.750	0.579	17	
	VGG19-Sagittal	0.568	0.480	0.280	0.680	0.447	0.486	19	
	VGG19-Combine	0.782	0.740	0.720	0.760	0.750	0.731	19	
	[Radiomics+VGG19]-Combine	0.760	0.680	0.360	1.00	1.00	0.610	19	11/19 (57.9%)
	Resnet-Axial	0.541	0.500	0.400	0.600	0.500	0.500	19	
	Resnet-Coronal	0.582	0.640	0.800	0.480	0.606	0.706	19	
	Resnet-Sagittal	0.662	0.580	0.400	0.760	0.625	0.559	19	
	Resnet-Combine	0.749	0.680	0.760	0.600	0.655	0.714	17	
	[Radiomics+Resnet]-Combine	0.811	0.720	0.640	0.800	0.762	0.670	16	10/16 (62.5%)
	Xception-Axial	0.528	0.520	0.200	0.840	0.556	0.512	19	
	Xception-Coronal	0.683	0.660	0.560	0.760	0.700	0.633	18	
	Xception-Sagittal	0.628	0.640	0.520	0.760	0.684	0.613	19	
	Xception-Combine	0.672	0.700	0.520	0.880	0.813	0.647	18	
	[Radiomics+Xception]-Combine	0.867	0.760	0.760	0.760	0.760	0.760	17	4/17 (23.5%)
	InceptionV3-Axial	0.529	0.600	0.760	0.440	0.576	0.647	18	
	InceptionV3-Coronal	0.533	0.460	0.400	0.520	0.455	0.464	19	
	InceptionV3-Sagittal	0.613	0.540	0.440	0.640	0.550	0.533	19	
	InceptionV3-Combine	0.707	0.660	0.600	0.720	0.682	0.643	16	
	[Radiomics+InceptionV3]-Combine	0.862	0.760	0.920	0.600	0.697	0.882	12	4/12 (33.3%)
	InceptionResnetV2-Axial	0.574	0.520	0.560	0.480	0.519	0.522	19	
	InceptionResnetV2-Coronal	0.602	0.540	0.160	0.920	0.667	0.523	18	
	InceptionResnetV2-Sagittal	0.702	0.520	0.040	1.00	1.00	0.510	19	
	InceptionResnetV2-Combine	0.686	0.600	0.320	0.880	0.727	0.564	19	
	[Radiomics+InceptionResnetV2]-Combine	0.849	0.740	0.680	0.800	0.773	0.714	19	7/19 (36.8%)
LR	Radiomics-Axial	0.811	0.740	0.720	0.760	0.750	0.731	14	
	Radiomics-Coronal	0.758	0.620	0.880	0.360	0.579	0.750	19	
	Radiomics-Sagittal	0.744	0.740	0.640	0.840	0.800	0.700	11	
	Radiomics-Combine	0.822	0.680	0.760	0.600	0.655	0.714	19	
	VGG16-Axial	0.690	0.640	0.600	0.680	0.652	0.630	14	
	VGG16-Coronal	0.710	0.720	0.600	0.840	0.789	0.677	18	
	VGG16-Sagittal	0.651	0.580	0.400	0.760	0.625	0.559	19	
	VGG16-Combine	0.692	0.600	0.480	0.720	0.632	0.581	19	
	[Radiomics+VGG16]-Combine	0.782	0.720	0.800	0.640	0.690	0.762	19	10/19 (52.6%)
	VGG19-Axial	0.669	0.600	0.520	0.680	0.619	0.586	19	
	VGG19-Coronal	0.704	0.660	0.600	0.720	0.682	0.643	19	
	VGG19-Sagittal	0.603	0.600	0.600	0.600	0.600	0.600	17	
	VGG19-Combine	0.597	0.540	0.400	0.680	0.556	0.531	17	
	[Radiomics+VGG19]-Combine	0.830	0.760	0.920	0.600	0.697	0.882	18	10/18 (55.6%)
	Resnet-Axial	0.602	0.580	0.520	0.640	0.591	0.571	19	
	Resnet-Coronal	0.566	0.560	0.640	0.480	0.552	0.571	19	
	Resnet-Sagittal	0.570	0.540	0.560	0.520	0.538	0.542	18	
	Resnet-Combine	0.508	0.500	0.560	0.440	0.500	0.500	18	
	[Radiomics+Resnet]-Combine	0.755	0.720	0.720	0.720	0.720	0.720	19	10/19 (52.6%)
	Xception-Axial	0.506	0.480	0.240	0.720	0.462	0.486	19	
	Xception-Coronal	0.651	0.660	0.480	0.840	0.750	0.618	19	
	Xception-Sagittal	0.632	0.620	0.520	0.720	0.650	0.600	17	
	Xception-Combine	0.678	0.600	0.320	0.880	0.727	0.564	17	
	[Radiomics+Xception]-Combine	0.712	0.700	0.560	0.840	0.778	0.656	19	4/19 (21.1%)
	InceptionV3-Axial	0.630	0.620	0.840	0.400	0.583	0.714	17	
	InceptionV3-Coronal	0.610	0.560	0.440	0.680	0.579	0.548	17	
	InceptionV3-Sagittal	0.682	0.680	0.440	0.920	0.846	0.622	19	
	InceptionV3-Combine	0.651	0.580	0.440	0.720	0.611	0.563	19	
	[Radiomics+InceptionV3]-Combine	0.688	0.580	0.520	0.640	0.590	0.571	18	3/18 (16.7%)
	InceptionResnetV2-Axial	0.450	0.420	0.080	0.760	0.250	0.452	14	
	InceptionResnetV2-Coronal	0.624	0.540	0.160	0.920	0.667	0.523	17	
	InceptionResnetV2-Sagittal	0.718	0.540	0.120	0.960	0.750	0.522	18	
	InceptionResnetV2-Combine	0.706	0.600	0.280	0.920	0.778	0.561	12	
	[Radiomics+InceptionResnetV2]-Combine	0.827	0.700	0.800	0.600	0.667	0.750	17	9/17 (52.9%)
Random Forest	Radiomics-Axial	0.742	0.640	0.560	0.720	0.667	0.621	15	
	Radiomics-Coronal	0.753	0.560	0.880	0.240	0.537	0.667	15	
	Radiomics-Sagittal	0.710	0.720	0.600	0.840	0.789	0.677	14	
	Radiomics-Combine	0.822	0.740	0.800	0.680	0.714	0.773	11	
	VGG16-Axial	0.674	0.700	0.520	0.880	0.813	0.647	15	
	VGG16-Coronal	0.734	0.680	0.760	0.600	0.655	0.714	19	
	VGG16-Sagittal	0.602	0.580	0.720	0.440	0.563	0.611	10	
	VGG16-Combine	0.712	0.600	0.680	0.520	0.586	0.619	19	
	Radiomics+VGG16	0.898	0.800	0.840	0.760	0.778	0.826	17	15/17 (88.2%)
	VGG19-Axial	0.649	0.580	0.560	0.600	0.583	0.577	15	
	VGG19-Coronal	0.675	0.580	0.840	0.320	0.553	0.667	18	
	VGG19-Sagittal	0.660	0.660	0.800	0.520	0.625	0.722	12	
	VGG19-Combine	0.734	0.680	0.760	0.600	0.655	0.714	17	
	[Radiomics+VGG19]-Combine	0.802	0.780	0.800	0.760	0.769	0.792	16	16/16 (100%)
	Resnet-Axial	0.604	0.580	0.240	0.920	0.750	0.548	11	
	Resnet-Coronal	0.621	0.580	0.600	0.560	0.577	0.583	12	
	Resnet-Sagittal	0.609	0.600	0.640	0.560	0.593	0.593	16	
	Resnet-Combine	0.626	0.640	0.520	0.760	0.684	0.684	12	
	[Radiomics+Resnet]-Combine	0.872	0.820	0.840	0.800	0.808	0.833	13	12/13 (92.3%)
	Xception-Axial	0.597	0.580	0.480	0.680	0.600	0.567	19	
	Xception-Coronal	0.702	0.620	0.720	0.520	0.600	0.650	16	
	Xception-Sagittal	0.657	0.600	0.720	0.480	0.581	0.632	13	
	Xception-Combine	0.746	0.680	0.840	0.520	0.636	0.636	11	
	[Radiomics+Xception]-Combine	0.819	0.780	0.800	0.760	0.769	0.792	13	10/13 (76.9%)
	InceptionV3-Axial	0.569	0.540	0.600	0.480	0.536	0.545	14	
	InceptionV3-Coronal	0.600	0.560	0.560	0.560	0.560	0.560	16	
	InceptionV3-Sagittal	0.610	0.600	0.640	0.560	0.593	0.593	15	
	InceptionV3-Combine	0.617	0.620	0.600	0.640	0.625	0.625	15	
	[Radiomics+InceptionV3]-Combine	0.806	0.780	0.920	0.640	0.719	0.889	19	14/19 (73.7%)
	InceptionResnetV2-Axial	0.551	0.540	0.440	0.640	0.550	0.533	17	
	InceptionResnetV2-Coronal	0.659	0.620	0.560	0.680	0.636	0.607	15	
	InceptionResnetV2-Sagittal	0.618	0.520	0.160	0.880	0.571	0.512	17	
	InceptionResnetV2-Combine	0.695	0.660	0.760	0.560	0.633	0.700	15	
	[Radiomics+InceptionResnetV2]-Combine	0.851	0.840	0.880	0.800	0.815	0.870	19	14/19 (73.7%)

LR, logistic regression; SVM, support vector machine; NPV, negative predictive value.

https://dx.doi.org/10.21037/qims-21-722

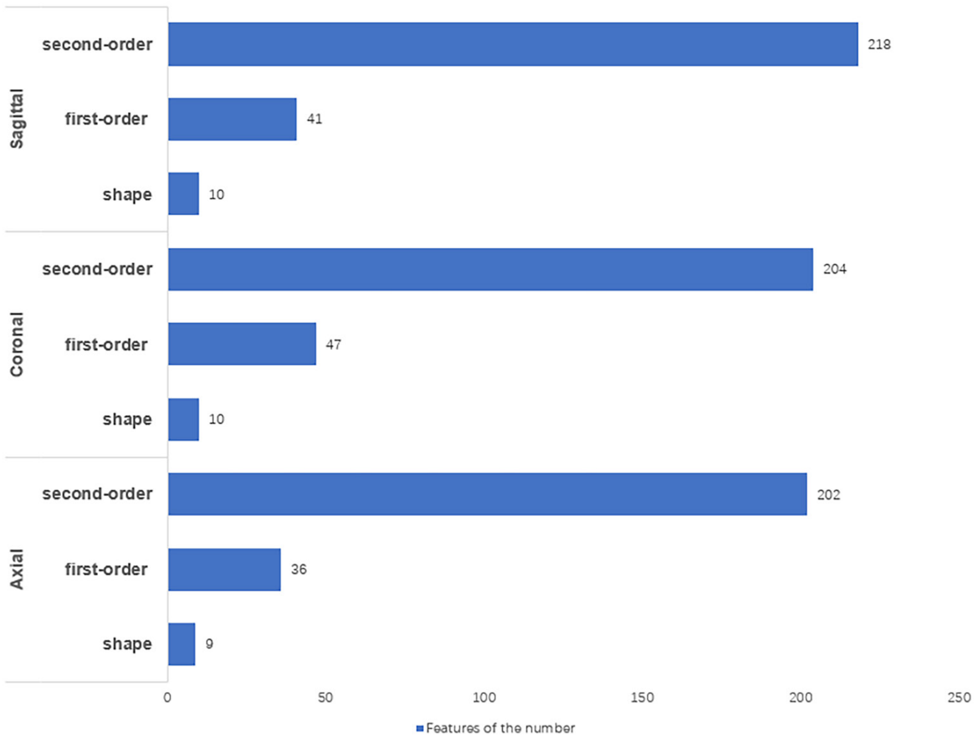

Figure S1 The remaining feature figures of axial, coronal, and sagittal images after removing redundant features by the Spearman correlation test.

References

47. Bengio Y, Grandvalet Y. No unbiased estimator of the variance of k-fold cross-validation. J Mach Learn Res 2004;5:1089-105.

 https://dx.doi.org/10.21037/qims-21-722